

The Multirotor Test Bed – A New NASA Test Capability for Advanced VTOL Rotorcraft Configurations

Carl Russell and Sarah Conley

Aeromechanics Office
NASA Ames Research Center
Moffett Field, CA

ABSTRACT

In November 2019, NASA completed the first wind tunnel test entry of the Multirotor Test Bed (MTB), a new test capability for advanced VTOL rotorcraft configurations. The MTB had been under development since 2017 when the need arose for an easily reconfigurable test stand for multirotor aircraft configurations. With the wide-ranging assortment of aircraft currently targeted at Urban Air Mobility and Unmanned Aircraft System applications, there is a need for validation data that will increase confidence in the computational modeling tools being used to develop these platforms. The MTB fills this need. This paper describes the key features of the MTB as well as its first wind tunnel test entry. A selection of results from the test is presented here, demonstrating the flexible configuration of the MTB and the types of data researchers can generate using this new test capability.

NOMENCLATURE

ESC	Electronic Speed Controller
MCS	MTB Control System
MTB	Multirotor Test Bed
MUAS	Multirotor Unmanned Aircraft System
PWM	Pulse-Width Modulation
TTL	Transistor-Transistor Logic
A	Rotor disk area, ft ²
C_P	Power Coefficient, $C_P = P/\rho A(\Omega R)^3$
C_T	Thrust Coefficient, $C_T = T/\rho A(\Omega R)^2$
dy	Lateral rotor spacing, ft
dz	Vertical rotor spacing, ft
P	Rotor power, hp
q	Dynamic pressure, lb/ft ²
R	Rotor radius, ft
ρ	Air density, slug/ft ³
Ω	Rotor rotational speed, rad/s

INTRODUCTION

The Multirotor Test Bed (MTB) is a new test capability recently developed by the Aeromechanics Office at NASA Ames Research Center with primary funding from the Revolutionary Vertical Lift Technology (RVLT) Project. The purpose of the MTB is wind tunnel and hover testing of arbitrary multirotor aircraft configurations with a focus on individual rotor loads data.

Because of the highly interactional nature of the airflow in multirotor systems, both steady and dynamic loads are of interest. In addition, the collection of acoustic data, where possible, is desired. The data collected will be used to validate simulations of multirotor systems and eventually lead to better predictions of multirotor performance.

Two previous wind tunnel tests of multirotor UAS vehicles were conducted in October-December 2015 [Ref. 1] and January-February 2017 [Refs. 2 and 3] – referred to as the MUAS1 and MUAS2 tests, respectively. The MUAS tests measured the aerodynamic performance of five quadcopters (3DR SOLO, 3DR Iris+, DJI Phantom 3 Advanced, SUI Endurance, and the ARL Overlapped Quadrotor), a tilt-wing (Elytron 4S UAV), and an octocopter (Drone America x8). The MUAS1 test entry generated a high-quality set of performance data for these vehicles and also raised additional questions, particularly related to vibrations, blade deflections, aerodynamic interference, acoustics, and trim strategies. The MUAS2 test expanded on the first by attempting to better characterize vibrations, interactional aerodynamics, and blade motion.

The MUAS tests had two main limitations:

- Loads were only measured for the entire vehicle, so a full picture of interactional aerodynamics could not be gleaned from the data
- Testing was limited to existing vehicles with no ability to alter the configuration

The MTB program built upon the knowledge gained during the MUAS tests. By measuring individual rotor loads for a multirotor system and allowing for adjustments to rotor position and attitude, the MTB will provide a wealth of data on the aeromechanics of arbitrary multirotor configurations.

Indeed, data collected during the first wind tunnel test entry are already being used to validate CFD predictions [Ref. 4]. This test capability will also be available for future tests of new multirotor aircraft concepts. The modularity of the MTB hardware was demonstrated in [Ref. 5], which used a large portion of the test rig hardware for a propeller test immediately following the MTB tunnel entry.

HARDWARE DESCRIPTION

An overview drawing of the MTB is shown in Figure 1, and Table 1 lists its capabilities. Figure 2 shows the MTB installed in the U.S. Army 7- by 10-ft Wind Tunnel at NASA Ames Research Center. Figure 3 shows a close-up photo of the rotor assembly hardware with the main components labeled. Figure 4 shows some of the key adjustable dimensions of the test rig. The full description of the MTB design is given in Ref. 6, but a short description is given here. The MTB consists of a strongback made of two 81-in long steel plates, between which are sandwiched six support blocks. The strongback is intended to support up to eight rotors, but for the first test entry, the maximum number of rotors was six. The strongback is supported by a single strut, and the pitch of the entire MTB is controlled via a pitch link that attaches to a jackscrew-actuated movable lug on the strut. The details of the pitch and tilt actuation are explained in the Control Systems section.

Up to four lateral support beams are attached to the strongback to support the rotors. These beams can be moved in the longitudinal direction to any of the hole locations on the strongback (provided the rotors don't interfere with each other). The lateral support beams have an "L-bracket" at each end, each consisting of a single machined piece of steel that slides over the lateral support beam to provide for lateral adjustment. A vertical support beam slides into the vertical leg of the L-bracket to provide for vertical adjustment of the rotor placement. A tilt mechanism using a linear actuator allows for adjustment of the rotor tilt between 90 degrees forward (airplane mode) and up to 5 degrees aft. The load cell, motor, and rotor are attached to the top of the tilt mechanism.

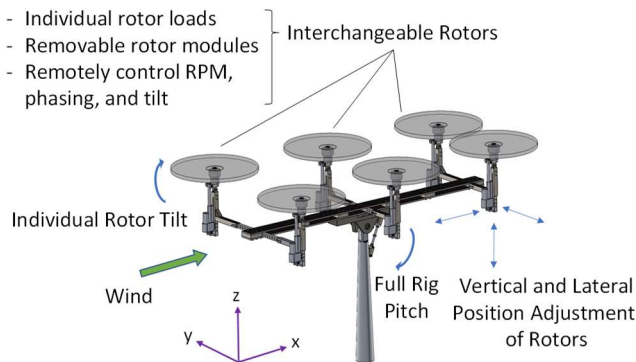


Figure 1. Overview of the Multirotor Test Bed

Table 1. MTB Capabilities and Limits

Characteristic	Range
Maximum rotor size	24.5 in (nominal size of the KDE-CF245-DP)
Maximum rotor RPM	4,500 (for 24.5 in rotor)
Lateral spacing	24.7 – 38.7 in, adjustable in 1 in increments (2 in if keeping symmetry about centerline)
Longitudinal spacing	25.5* – 72 in, adjustable in 1.5 in increments
Vertical position	9 in of travel, adjustable in 1 in increments
Individual rotor tilt	90 deg forward to 5 deg aft, adjustable in arbitrary increments
Full MTB pitch	20 deg nose down to 10 deg up, adjustable in arbitrary increments
Maximum wind speed	40 ft/s, for initial testing; more if vibratory loads are low enough

* Minimum when 24.5-in rotors are installed; less if rotor diameter is smaller



Figure 2. MTB installed in the U.S. Army 7- by 10-ft Wind Tunnel

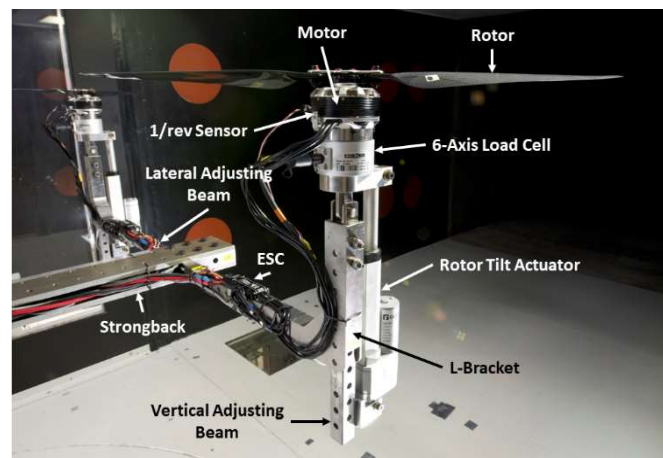


Figure 3. MTB rotor assembly detail

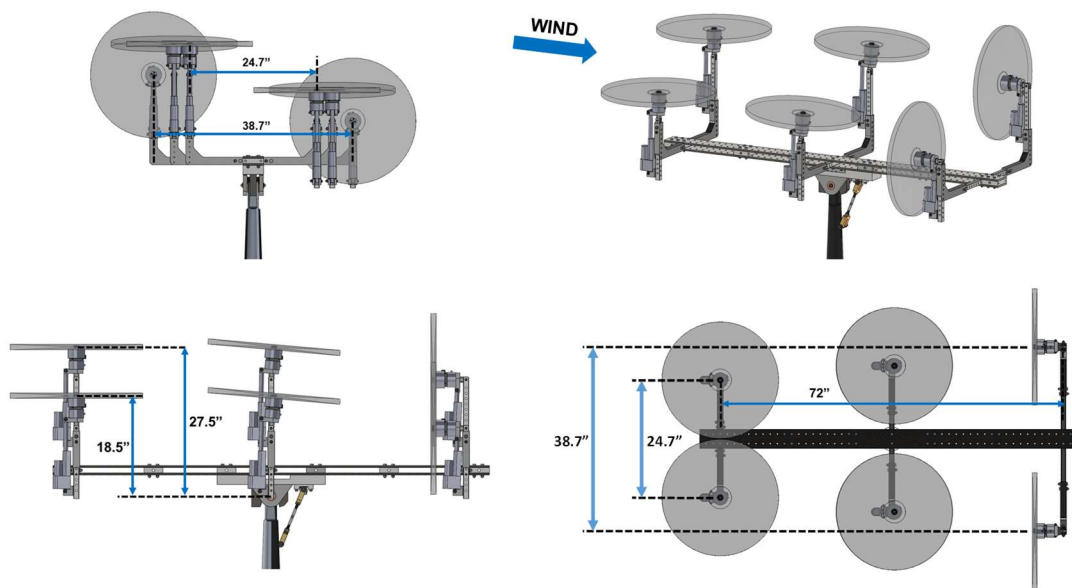


Figure 4. Different views of the MTB showing key adjustable dimensions

CONTROL SYSTEMS

The MTB allows independent remote control of all six rotors, both in rotor speed and in rotor tilt. Additionally, the pitch of the entire MTB can be adjusted by the model operator from the wind tunnel control room. The following sections describe the systems used for control of these different variables.

MTB Control System

The MTB is controlled by a LabView program called the MTB Control System (MCS). The MCS controls and monitors all electronic functions of the MTB, including main bus power and temperature, rotor speed, rotor tilt, and MTB pitch. Various peripherals, described in subsequent sections here, are used to drive the different actuators.

The MCS communicates through a National Instruments data acquisition board with the different peripheral systems over serial communication lines. The pitch, tilt, and rotor speed controllers are all made by Pololu Robotics & Electronics. These different Pololu systems have the ability to send and receive messages over two TTL serial lines using a command protocol called simply the “Pololu protocol.” The complete details of the Pololu protocol are beyond the scope of this paper, but the basic functionality of the protocol is that a set of command bytes are encoded along with a device identifier, which allows multiple devices to listen and receive commands on the same line. The Pololu devices are also able to communicate back to the MCS via a transmit line.

From a cabling perspective, this system is very lightweight, as it only requires a single three-conductor instrumentation cable to simultaneously communicate with many different

devices. The system is, however, fairly limited in bandwidth compared with other serial protocols, such as USB and RS-232. For practical purposes on the MTB, the maximum baud rate was 10,000 bits per second, which limited the refresh rate of the control inputs to approximately 2/sec. In the six-rotor configuration, this update rate was sufficient, but may not be satisfactory if more rotors are added to the MTB.

Rotor Speed

The rotor speed on the MTB is controlled by off-the-shelf KDE electronic speed controllers (ESCs). As with other commercial ESCs, those used for the MTB receive a pulse-width-modulated signal, similar to that used for a radio-controlled aircraft servo. A Pololu Mini Maestro 12-channel servo controller provides the PWM signals to the six individual speed controllers. The Mini Maestro is a low-cost device that was previously used for the successful Multirotor UAS tests conducted in the 7- by 10-ft Wind Tunnel in 2015 and 2017 [Ref. 1]. It communicates with the MCS over serial lines using the methods described in the previous section. This setup requires very little cabling between the MCS and the model, making the system fairly portable. This portability will be an advantage if there is a desire in the future to use the MTB in a different wind tunnel facility where the cable run lengths may be different between the test section and control room.

The motor speed on the MTB is measured using an infrared optical sensor that provides a 1/rev pulse train. This signal is captured by the MCS and processed into rotor RPM by measuring the time between pulses. In practice, these RPM measurements were found to be accurate to within

approximately 2 to 3 rpm, representing a maximum RPM measurement error of 0.2% at the minimum rotor speed of 1,500 rpm.

A simple feedback controller was built using LabView's built-in PID control function. The controller was tuned initially with the Ziegler-Nichols method, but this led to an overly-sensitive RPM response. The controller gains were then refined through trial and error until satisfactory performance was achieved. The controller as currently implemented can maintain rotor speed to within approximately 10 rpm.

Rotor Tilt

The tilt angles of the individual rotors on the MTB are controlled by electric linear actuators. These actuators use a potentiometer to provide analog feedback proportional to the actuator position. A Pololu JRK G2 Motor Controller is connected to each actuator. Like the RPM control system, communication from the MCS to the motor controller is implemented via the Pololu protocol over a TTL serial line. The potentiometer feedback is constantly queried by the MCS and reported to the model operator.

There is no direct measurement of rotor tilt on the MTB. Instead, the linear actuator position for each rotor has been mapped to an angle using a precision hand-held inclinometer. This angle mapping has been programmed into the MCS so the operator can command a tilt angle, and the actuator will move to the corresponding extension length. It is also worth noting that the rotor tilt angle does not require the linear actuators to be powered in order to hold position. The gearing of the actuators is configured such that they cannot be back-driven. The MTB pitch angle, described in the next section, has this same characteristic, which is a useful safety feature that limits the potential consequences of any actuator power failure.

MTB Pitch

As described in the MTB hardware section, the pitch of the entire MTB is actuated by a jackscrew connected to a pitch link on the mounting strut. The jackscrew is turned by a small stepper motor that transmits power through an attached 9:1 reduction gearbox. The resulting pitch actuation is very slow (a few seconds per degree), but allows for control of the pitch angle with only a 10-watt stepper motor.

A Pololu Tic T825 Stepper Motor Controller provides both the drive power and the control function for the pitch stepper motor. Similar to the RPM controller and the tilt controller, the Tic receives Pololu protocol commands over a TTL serial line and transmits current status back to the MCS.

An analog inclinometer is secured to the upper surface of the MTB strongback to provide a direct measurement of the pitch

angle. This angle is displayed on the operator console of the MCS, but there is no closed-loop control. The operator enters a step count that roughly corresponds to the desired pitch angle and then subsequently fine-tunes the angle. This procedure is a bit labor intensive, but in practice, there aren't many pitch angle changes during any given data run, so the process did not significantly hinder testing. Future modifications to the MTB may include closed-loop control of the pitch angle.

Power Systems

There are two main power systems for the MTB. The primary power for the rotors is provided by a 5 kW DC power supply that generates a maximum current of 100 A at up to 50 V. For this test, the main rotor power was supplied at 48 V. The power limit of 5 kW is dictated by the available wall power in both the NASA model prep facility and in the wind tunnel.

The output of the primary power supply is controlled by the MCS via an RS-232 serial line. The current limit and voltage can be remotely set by the model operator from the MCS, and the output of the power supply can also be remotely switched on and off. In addition to the manual cutoff at the model operator station, the output of the power supply is interlocked to the wind tunnel test section doors, removing the possibility of powering the model with a person in the test section.

Power is distributed to the rotors through a power bus mounted on the MTB strongback. The power bus has connections for 8 rotors, but for this test, only 6 of the power bus outputs were used. The bus contains two large diodes to protect the power supply from voltage spikes. Since these diodes generate a significant amount of heat, active cooling is provided by fans in the power bus case. The diode temperatures are measured by two thermocouples and are constantly monitored in the MCS.

The second power system is a 12 V DC power supply, which provides power to the pitch and tilt actuators as well as to the Pololu control hardware and the pitch-sensing inclinometer. All of the 12 V hardware is relatively low current and does not have much potential for causing damage in the event of a malfunction, so no remote control or interlock is implemented for this hardware. There is an emergency stop button at the operator console, so power can be immediately cut to all of the 12 V hardware in the event of an emergency or mishap.

Measurement Systems

The primary measurements of interest on the MTB are the individual rotor loads. Each rotor sits on top of a 6-axis load cell capable of measuring both steady and dynamic loads. The load cells used on the MTB are Interface model 6AR70A-S11, with a capacity of 75 lb in all three force directions and 115 in-lb in all three moment directions.

The Interface load cells are paired with Interface Model BX8-HD44 amplifiers that combine the signals from the strain gauges in the load cell assembly and resolves them into six analog signals proportional to each of the six primary forces and moments. The amplifier also provides automatically configured low-pass filtering for a maximum sample rate of 12,000/s. For this test, the maximum frequency of interest corresponded to 12/rev at 4,500 rpm, or 900 Hz. The amplifier filter was set to a cutoff frequency of 2 kHz. The resolved analog signals are sent to the wind tunnel data system, which, for this test, was set to a sample rate of 4,000 samples per second.

In addition to the load cell measurements, overall loads on the MTB were measured using the wind tunnel’s external scales. Unlike the load cells, the scales are only capable of measuring steady loads. The overall MTB loads were not particularly of interest for this test, because the only components being tested were the rotors. If a wing or fuselage is added to the MTB in the future, the tunnel scales could measure the additional loads on these static components. For this test, the scales merely provided validation of the load cell data.

The force and moment measurements are the only scientific data reported in this paper. Acoustic data were also recorded using a phased microphone array system similar to that described in Ref. 7, and those data are still being processed. Other data recorded by the data system included the model state (motor RPM, rotor tilt, MTB pitch) and wind tunnel conditions (such as speed, density, temperature, etc.).

TEST DESCRIPTION

Test Objectives

The test performed in late 2019 was the first wind tunnel entry for the Multirotor Test Bed. As such, a main focus of the test was ensuring that the MTB could successfully perform all of its designed functions while installed in the 7- by 10-ft Wind Tunnel. The primary systems checked out and used for this test entry were:

- MTB control systems, including individual rotor tilt, full pitch of the MTB, and rotor RPM control
- MTB hardware, including the strongback assembly, vertical and lateral adjusting beams, and pitch and tilt mechanisms
- Force measurement systems, primarily consisting of the six-axis load cells located at the base of each of the MTB motors.

The primary scientific objective of the MTB project was the measurement of forces and moments experienced by the individual rotors of a multirotor system. In so doing, the highly interactional aerodynamics of multirotor systems were explored. One specific type of test that was targeted by the

MTB project was to measure the effect of relative vertical placement of the forward and aft rotors in a quadrotor configuration. Previous studies have shown that there is an optimal vertical separation of the forward and aft rotors, and this test sought to support that conclusion with experimental data [Ref. 8]. In broad strokes, the main research goal of the MTB is to provide experimental data to help validate computational performance predictions for multirotor aircraft.

Test Matrix

The primary purpose of the first wind tunnel test entry was demonstrating the capabilities of the MTB. In particular there was a desire to show that the test rig could be rapidly reconfigured while retaining all of its measurement capabilities. The test matrix was a reflection of the desire to exercise as many of the configuration capabilities as possible within the test window. It is expected that future tests would have a narrower focus and would more specifically target individual parameter sweeps, such as rotor spacing. The test matrix is summarized in Table 2. For all test conditions, both weight and aerodynamic tare data were collected and applied during post-processing. Note that not all possible combinations shown in Table 2 were tested. Generally, the parameter sweeps included the following values:

- Pitch, defined positive nose up: -10, -5, -2, 0, 2, 5 deg
- Tilt, defined positive nose down relative to the strongback, with 0 deg representing the rotor plane parallel to the strongback (helicopter mode): -5, -2, 0, 2, 5, 10, 30, 45, 60, 90 deg
- Yaw, defined positive nose right: -10, -5, -2, 0, 5, 10 deg
- Rotor speed: 1,500 to 3,500 rpm, in increments of 500

The full test matrix and results from this wind tunnel test will be documented in a NASA Technical Memo at a later date.

Because there are so many ways of positioning the rotors, a generalized numbering convention was used to describe the rotor positions. This numbering convention assumes bilateral symmetry across the MTB centerline. For a more general description of the rotor positioning that does not require symmetry, a different numbering scheme would have to be adopted. The rotor positioning is given by three ordered triples:

$$\begin{pmatrix} P_{1x} & P_{2x} & P_{3x} \\ P_{1y} & P_{2y} & P_{3y} \\ P_{1z} & P_{2z} & P_{3z} \end{pmatrix}$$

The first subscript indicates the row of rotors – the numbers 1, 2, and 3 correspond to the forward, middle, and aft rotors respectively. The second subscript refers to the positioning direction, with x , y , and z referring to the longitudinal, lateral,

and vertical positions, respectively. The positions are given in terms of bolt-hole locations which are described here:

- Longitudinal, or x -position: numbered from 0 to 48. 0 is the forward-most position, while 48 is the aft-most position. The longitudinal positioning bolt holes are spaced at 1.5-in increments, with a maximum spacing of 72 in.
- Lateral, or y -position: numbered from 0 to 7. 0 is the inner-most position, while 7 is the outer-most position. The lateral positioning bolt holes are spaced at 1.0 in increments, with a maximum spacing of 38.7 in.
- Vertical, or z -position: numbered from 0 to 9. 0 is the lowest position, while 9 is the tallest position. The vertical positioning bolt holes are spaced at 1.0 in increments. For practical purposes, 7 is the highest position that can be used for the 7- by 10-ft Wind Tunnel installation. Positions 8 and 9 would place the rotors too close to the ceiling at certain rotor tilt angles, presenting both a safety concern

and potential data quality issues due to wall effects on the rotor inflow.

While there was not a narrowly targeted engineering question addressed by this test, several parameters were systematically investigated including the following:

- The effects of the presence of multiple rotors, by investigating single-rotor performance, plus two-, four-, and six-rotor configurations under the same tunnel conditions and rotor settings.
- The effects of lateral spacing on two side-by-side non-overlapping rotors. As an aside, the effects of lateral spacing on side-by-side overlapping rotors are currently being investigated in another NASA test program.
- The effects of fore-aft vertical rotor spacing on a quadrotor configuration.
- The effects of RPM and tilt transients.

Table 2. MTB Wind Tunnel Test Matrix

Rotor Positions	Rotors Installed						Pitch Angles (deg)	Tilt Angles (deg)	Yaw Angles (deg)	Rotor Speeds (rpm)	Nominal Wind Speeds (ft/s)
	1	2	3	4	5	6					
$\begin{pmatrix} 0 & 24 & 48 \\ 7 & 7 & 7 \\ 7 & 7 & 7 \end{pmatrix}$	X	X	X	X	X	X	-10 to +10	0	-10 to +10	1,500 to 3,000	20, 40
	X	X	X	X	X	X	-5, 0	-5 to +90	0	2,000	20
	X	X	X	X	X	X	-10 to +5	0	0	1,500 to 3,000	20, 40
	X	X	X	X			-10 to +5	0	0	1,500 to 3,000	20
$\begin{pmatrix} 0 & 24 & 48 \\ 7 & 7 & 7 \\ 0 & 0 & 0 \end{pmatrix}$	X	X	X	X			0	-5 to +90	0	2,000	20
				X			-10 to +5	0	0	1,500 to 3,500	20, 40
							-10 to +5	0	0	1,500 to 3,500	20, 40
				X			0	-5 to +90	0	2000	20
		X					-10 to +5	0	0	1,500 to 3,500	20, 40
			X				-2, 0	0	0	2,000, 3,000	20
$\begin{pmatrix} 0 & 24 & 48 \\ 7 & 7 & 7 \\ 0 & 7 & 0 \end{pmatrix}$	X	X	X	X			-10 to +5	0	0	1,500 to 3,500	20, 40
	X	X	X	X			0	-5 to +90	0	2,000	20, 40
$\begin{pmatrix} 0 & 24 & 48 \\ 4 & 7 & 7 \\ 0 & 7 & 0 \end{pmatrix}$	X	X	X	X			-10 to +5	0	0	1,500 to 3,500	20, 40
	X	X	X	X			0	-5 to +90	0	2,000 to 4,000	20, 40
	X	X					-2, 0	0	0	1,500 to 3,500	20, 40
$\begin{pmatrix} 0 & 24 & 48 \\ 1 & 7 & 7 \\ 0 & 7 & 0 \end{pmatrix}$	X	X					-10 to +5	0	0	1,500 to 3,500	20, 40
	X	X					0	-5 to +90	0	2,000 to 4,000	20, 40
		X					-2, 0	0 to +45*	0	1,500 to 2,500*	20, 40
$\begin{pmatrix} 0 & 24 & 48 \\ 1 & 7 & 1 \\ 0 & 0 & 0 \end{pmatrix}$	X	X	X	X	X	X	-10 to +2	0	0	1,500 to 3,500	20, 40
	X	X	X	X	X	X	0	-5 to +90* [†]	0	2,000	20, 40

* Sweeps included transients

[†] Sweeps included tilting just Rotors 3 and 4 with the others remaining at 0 deg

RESULTS

The following section presents a small subset of the data that were collected during the first test entry of the Multirotor Test Bed. The complete data set will be published at a later date in a NASA Technical Memo.

Throughout this section, the rotors are referred to by their rotor number, from 1 to 6. Figure 5 shows a top-down view of the MTB with the rotors identified by number. It also indicates the rotation direction of each rotor.

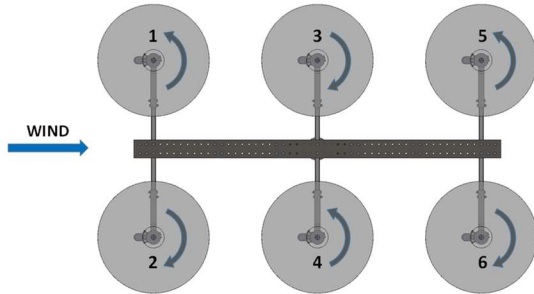


Figure 5. MTB rotor numbering and rotation directions

Data Caveats

There are a couple of caveats on the data presented here, and values in the plots should not be interpreted as final results, but rather as representative of the type of data that can be generated with the MTB. These deficiencies will be corrected before the complete results are published in the final data report.

The loads data presented here are based on a calibration that was provided by the load cell manufacturer. During instrumentation checkouts, discrepancies were found between known check loads and the data obtained from the load cells. Troubleshooting the instrumentation led to the conclusion that the calibration matrix was inaccurate, but there was insufficient time to re-calibrate prior to the wind tunnel entry. A post-test calibration of the six-axis load cells and re-reduction of the data are planned, but these activities have been delayed due to COVID-19-related facility access restrictions.

The other main caveat on the data is that the wall effects of the wind tunnel are still being investigated. Ref. 4 has shown that the impacts of the walls are non-negligible for the MTB. Further investigation of these impacts is warranted, and will likely require corrections similar to those given in Ref. 9.

Effects of Multiple Rotors

The main strength of the Multirotor Test Bed is its ability to generate independent loads for each of the rotors. The data presented in this section demonstrate the different results obtained with 1, 2, 4, or 6 rotors installed on the MTB.

Figures 6-9 show the thrust and power on Rotor 3 for a dynamic pressure of 0.48 lb/ft^2 and rotor speed of 2,000 rpm. Recall from Fig. 5 that Rotor 3 is the middle, right-hand rotor when looking at the MTB from above. Also note that there was no effort made to achieve any kind of trim, because the MTB is not representing an aircraft in this test case. The thrust and power therefore represent the measurements that result from holding the desired rotor speed and attitude.

The thrust is shown in Fig. 6 in dimensional units and in coefficient form in Fig. 7. The differences between the isolated rotor and side-by-side cases are fairly minor, with the side-by-side case resulting in a slightly higher thrust on Rotor 3. Once the front rotors (Rotors 1 and 2) are added, there is a significant drop-off in the thrust produced by Rotor 3, as it becomes impacted by the wake of the front two rotors. Adding

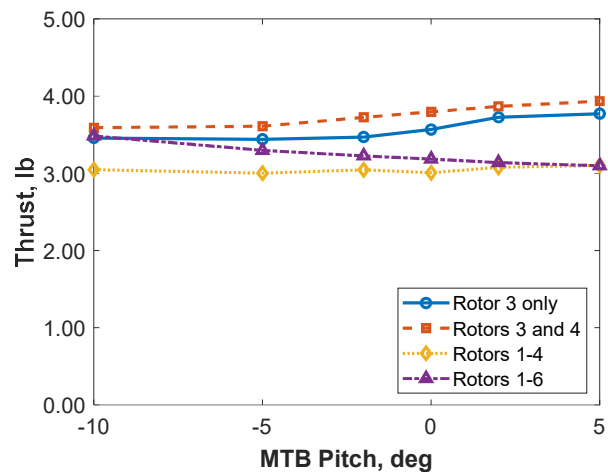


Figure 6. Thrust for Rotor 3 with different numbers of rotors present at varying angle of attack. RPM = 2,000, and $q = 0.48 \text{ lb/ft}^2$.

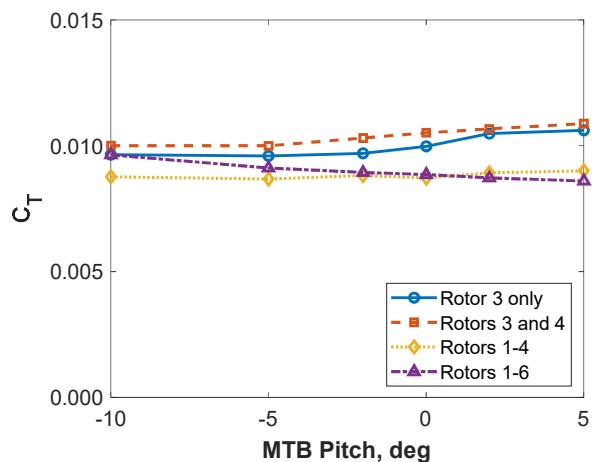


Figure 7. Thrust coefficient for Rotor 3 with different numbers of rotors present at varying angle of attack. RPM = 2,000, and $q = 0.48 \text{ lb/ft}^2$.

the aft two rotors (Rotors 5 and 6) apparently decreases this effect at nose-down pitch angles, with the thrust nearly matching the isolated rotor and side-by-side cases. At more horizontal or positive pitch angles, the results approach those seen in the 4-rotor case.

Results for the rotor power are shown in Figs. 8 and 9 in dimensional and non-dimensional units, respectively. For power, the isolated rotor and side-by-side cases match each other almost identically. Once the forward rotors are added, the power required to maintain 2,000 rpm on Rotor 3 increases. Except at the highest angle of attack, the measured power on Rotor 3 is nearly identical between the 4- and 6-rotor cases. The power measured in horsepower is noticeably lower for the 4-rotor case, but this discrepancy disappears once the effects of density are removed by the power

coefficient calculation. The remaining mean loads data presented in this section are expressed only in coefficient form.

The next four plots (Figs. 10 – 13) show the variation in measured thrust and power between the different rotors when all six rotors are installed. Figures 10 and 11 show the variation in thrust and power coefficient with all six rotors operating at 2,000 rpm and a wind tunnel dynamic pressure of 0.48 lb/ft². In general, it can be observed that the front rotors draw slightly less power and produce slightly more thrust than the middle and aft rotors. This effect is likely due to the middle and aft rotors operating in the wake of the forward rotors. This result is consistent with the trends observed in Figs. 7 and 9.

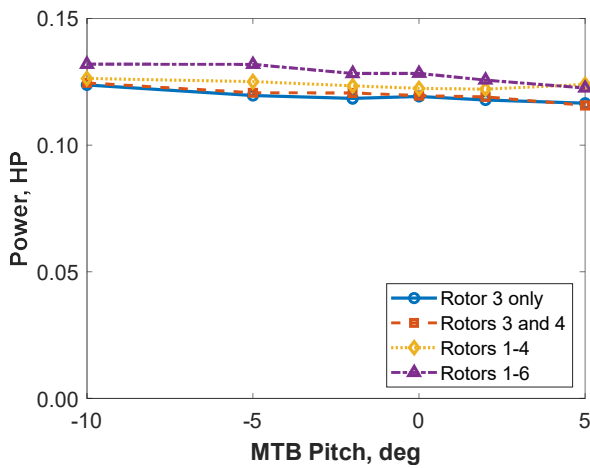


Figure 8. Power for Rotor 3 with different numbers of rotors present at varying angle of attack. RPM = 2,000, and $q = 0.48 \text{ lb/ft}^2$.

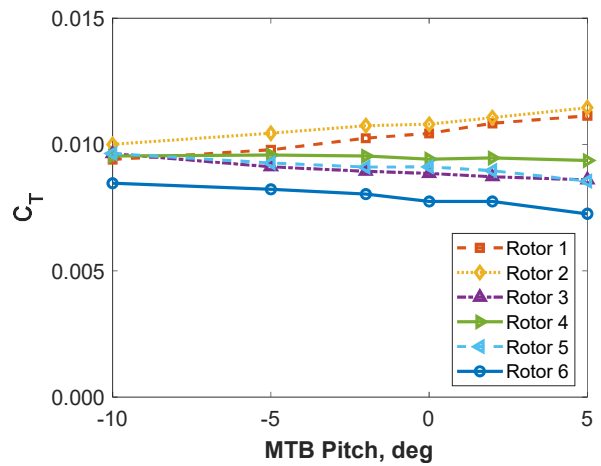


Figure 10. Thrust coefficient for each rotor with six rotors present at varying angle of attack. RPM = 2,000, and $q = 0.48 \text{ lb/ft}^2$.

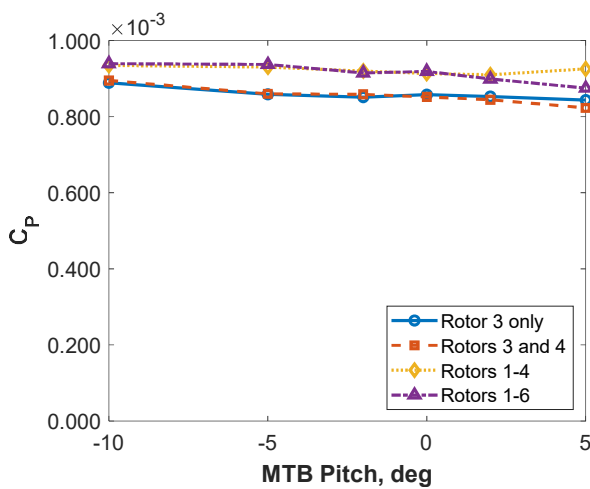


Figure 9. Power coefficient for Rotor 3 with different numbers of rotors present at varying angle of attack. RPM = 2,000, and $q = 0.48 \text{ lb/ft}^2$.

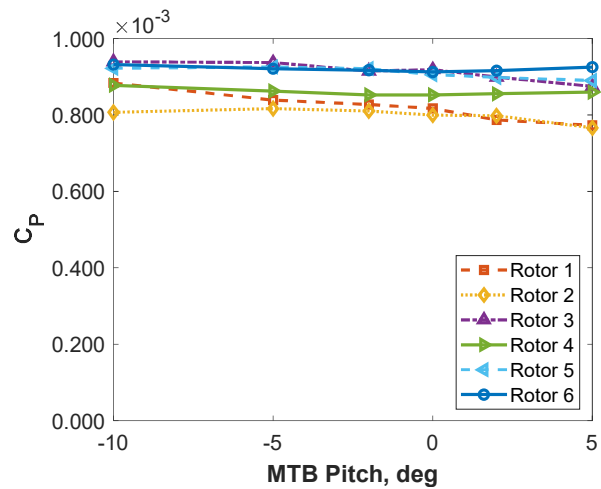


Figure 11. Power coefficient for each rotor with six rotors present at varying angle of attack. RPM = 2,000, and $q = 0.48 \text{ lb/ft}^2$.

One curious observation in Figs. 10 and 11 is the poor agreement in loads between Rotors 3 and 4 as well as between Rotors 5 and 6. Because the MTB was operating in a symmetric configuration in this case, one would expect the left and right rotors at the same longitudinal station to exhibit nearly identical results. This discrepancy is being investigated and may be related to the data caveats discussed previously.

Figures 12 and 13 show the variation in thrust and power coefficient with all six rotors operating at 2,000 rpm and a wind tunnel dynamic pressure of 1.9 lb/ft². In this case, the differences between the forward, middle, and aft rotors are more readily apparent. As seen in the lower-speed case, the forward rotors generate more thrust and draw less power than the middle and aft rotors. There is again a discrepancy

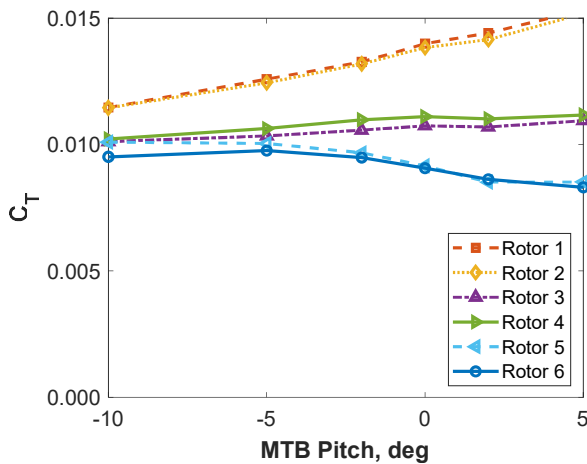


Figure 12. Thrust coefficient for each rotor with six rotors present at varying angle of attack. RPM = 2,000, and $q = 1.90 \text{ lb/ft}^2$.

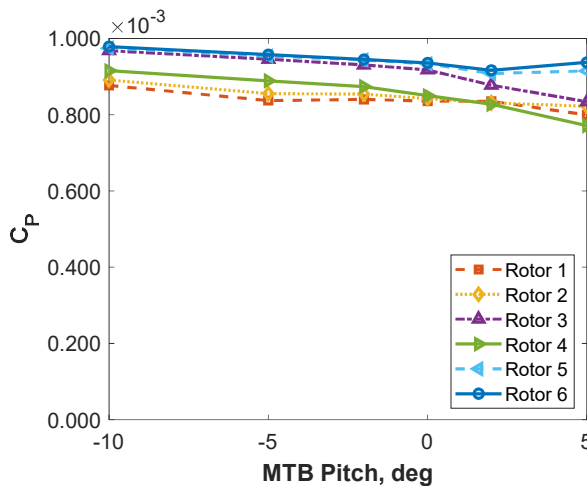


Figure 13. Power coefficient for each rotor with six rotors present at varying angle of attack. RPM = 2,000, and $q = 1.90 \text{ lb/ft}^2$.

between the power coefficient for Rotors 3 and 4, similar to the $q = 0.48 \text{ lb/ft}^2$ case. The thrust coefficient, on the other hand, is well matched between the left and right rotors at each longitudinal station for the $q = 1.9 \text{ lb/ft}^2$ case. The more pronounced differences in thrust values for the higher speed case is almost certainly due to the higher wake skew angle that would be expected at higher speed, leading to a stronger interference effect between longitudinally spaced rotors.

Effects of Rotor Spacing

The next sets of results demonstrate the types of studies that can be performed using the MTB to reconfigure the rotor-to-rotor spacing. The first set of charts shows the effects of lateral spacing on rotor thrust and power, while the second set shows the effects of vertical spacing.

Figures 14 and 15 show the thrust and power coefficients measured for the right-hand rotor at three different values of lateral spacing. The results show data for either Rotor 1 or 3 because the different 2-rotor configurations weren't all run with the same side-by-side pair). The positions of the rotors are 1 (inner-most), 4 (middle), and 7 (outer-most). These three positions correspond to a lateral spacing of 26.7, 32.7, and 38.7 in, or $dy/R = 2.18, 2.67, \text{ and } 3.16$, respectively. Hole-position 1 is actually not the inner-most location that a rotor on the MTB can be located, but with a rotor diameter of 24.5 in, mounting the rotors at hole-position 0 would leave just 0.2 in between blade tips. This small clearance was judged to be too close for safe operation, but with a smaller-diameter rotor, this inner bolt-hole location could be safely used.

Adding to the comparison between the single rotor and the two side-by-side rotors shown earlier in Fig. 7 and 9, Figs. 14 and 15 show that moving the two rotors closer together results in more thrust being produced at lower power for the same wind and rotor speeds. The MTB does not have mechanical rotor synchronization, so investigating intermeshing side-by-side rotors is not feasible; however, another NASA experiment on a different test stand will investigate the performance of intermeshed side-by-side rotors later in 2020.

The final results presented here for mean rotor loads show the effects of adjusting the vertical separation between forward and aft rotors on a quadrotor configuration. Figures 16 and 17 show power and thrust for the forward and aft right-hand rotors (Rotors 1 and 3, respectively). The two configurations shown are with all four rotors at the lowest possible location ($dz/R = 0$) and with the aft two rotors at the highest possible location ($dz/R = 0.57$). In both configurations, the rotor speed on all four rotors is 2,000 rpm, and the tunnel dynamic pressure is 0.48 lb/ft^2 .

For the case with all four rotors at the same height, there is a large separation between the results for the forward and aft rotor for both C_P and C_T . Clearly, there is a large interference

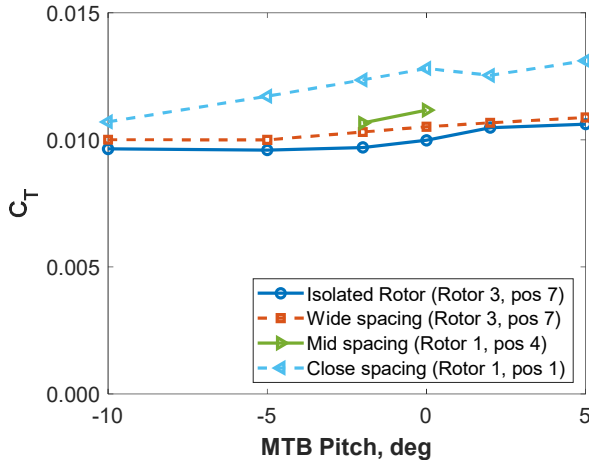


Figure 14. Thrust coefficient for the right-hand rotor with two rotors present at different lateral spacing and varying angle of attack. RPM = 2,000, and $q = 0.48 \text{ lb/ft}^2$.

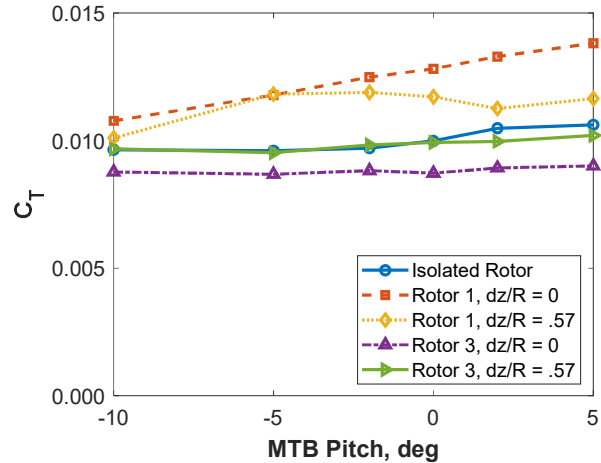


Figure 16. Thrust coefficient for the right-hand rotors with four rotors present at different vertical spacing and varying angle of attack. RPM = 2,000, and $q = 0.48 \text{ lb/ft}^2$.

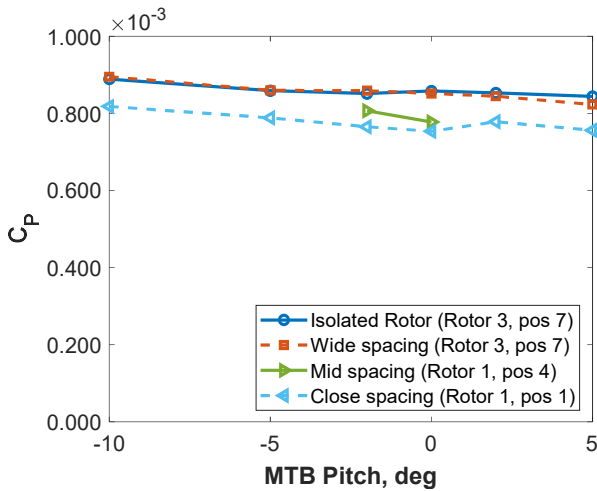


Figure 15. Power coefficient for the right-hand rotor with two rotors present at different lateral spacing and varying angle of attack. RPM = 2,000, and $q = 0.48 \text{ lb/ft}^2$.

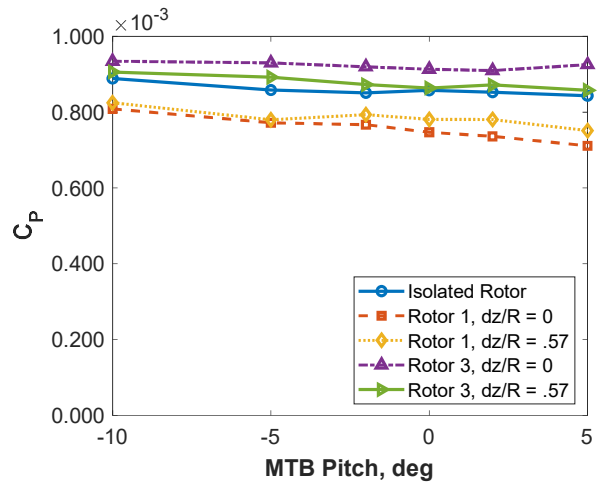


Figure 17. Power coefficient for the right-hand rotors with four rotors present at different vertical spacing and varying angle of attack. RPM = 2,000, and $q = 0.48 \text{ lb/ft}^2$.

effect between the forward and aft rotors that increases the power and decreases the thrust produced by the aft rotors. When the vertical separation is increased, the power required by the aft rotor decreases, while its thrust increases. With the increased vertical separation, the aft rotors' performance nearly matches that of the isolated rotor. This is a similar result to those observed in CFD predictions for the MTB presented in Ref. 4, as well as in previous computational studies on other multirotor configurations, such as those presented in Refs. 10 and 11. At the same time, the forward rotor becomes less efficient, producing less thrust at a higher power level than for the $dz/R = 0$ case.

This and the previous examples do not represent trimmed aircraft configurations, so additional studies would be needed

to investigate the effects of spacing and rotor placement on actual vehicle performance. These results are given to show the types of data and trade studies that could potentially be explored using the MTB.

Dynamic Loads

The previous sections dealt with the results for mean loads, which are obtained by sampling the load cells at 4 kHz for 30 seconds and averaging the data. This section shows sample results for dynamic loads data obtained from the six-axis load cells. For every data point collected, both mean loads and a 5-second sample of the dynamic loads were collected for all 36 load cell channels. For the transient cases, the dynamic data collection time window was increased as necessary.

Figure 18 shows the vibratory loads in the x-direction for Rotor 3 both in isolation and in a six-rotor configuration (the same test points as those shown in Figs. 6-11). The vibratory loads are expressed at discrete harmonics of the rotor rotational speed, or N/rev. In the previous MUAS tests with 2-bladed rotors, described in Refs. 1 and 2, high vibratory loads were observed, especially at 2/rev. A similar trend was observed with the MTB, which is not surprising given that its rotors are also 2-bladed.

The isolated rotor case shows very high 2/rev loads, but the loads at the remaining harmonics are nearly an order of magnitude less. In the 6-rotor case, the 2/rev loads are still quite high, but the 4/rev loads are also significant, indicating blade-wake interactions between the rotors. One area of planned future research on the MTB is an investigation of the effects of rotor azimuth phasing on the vibratory loads. Research has already shown that there are acoustic advantages to controlling rotor phasing [Ref. 12], and it is reasonable to expect that vibratory loads could be reduced using similar methods. Thus far, however, the MTB control system is not capable of controlling the rotor-to-rotor phasing. The uncontrolled rotor phase tends to meander at a given rotor speed, which leads to time-varying vibration magnitudes.

Another function the MTB is capable of is creating rotor speed transients, which can be investigated for their effects on rotor loads. Figure 19 shows the thrust response of an isolated rotor undergoing a transient from 1,500 to 2,500 rpm at a dynamic pressure of 1.9 lb/ft² and an MTB pitch angle of -2 deg. As shown, the vibratory thrust loads are quite high, with approximately the same magnitude as the mean load. The red line shows a rolling average of the thrust, while the yellow line, plotted against the secondary axis, shows the rotor RPM. One thing that can be observed in Fig. 19 is that the thrust change appears to lag slightly behind the rotor speed change. This effect is not unexpected, as the rotor wake takes a finite amount of time to respond to the change in rotor speed. Understanding the rotor load and vehicle response to changes in RPM is an active area of research at NASA [Ref. 13], and this type of transient data could provide validation data for these efforts.

Finally, Fig. 20 shows a waterfall plot for the same transient thrust data shown in Fig. 19. In this image, the 2, 4, 6, and 8/rev harmonics are clearly visible, with 2/rev being the most prominent. The remaining harmonics are present, but are at a much lower magnitude.

SUMMARY AND CONCLUSIONS

The Multirotor Test Bed is a new capability for multirotor testing developed at NASA Ames Research Center. The goal of the MTB project was to create a testbed that could be used for studies of advanced VTOL rotorcraft configurations,

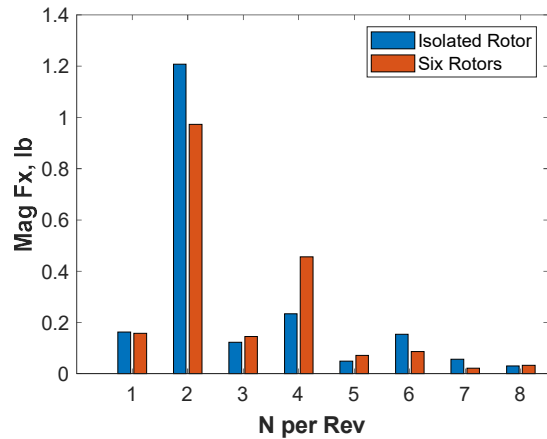


Figure 18. Rotor 3 N/Rev vibratory loads in the x-direction, in isolation and with all six rotors present. RPM = 2,000, and $q = 0.48$ lb/ft².

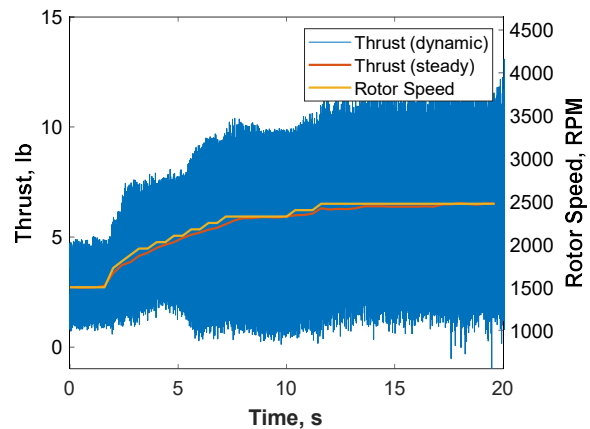


Figure 19. Rotor 2 isolated rotor thrust response to an RPM transient from 1,500 to 2,500 rpm. Pitch = -2 deg, and $q = 1.9$ lb/ft².

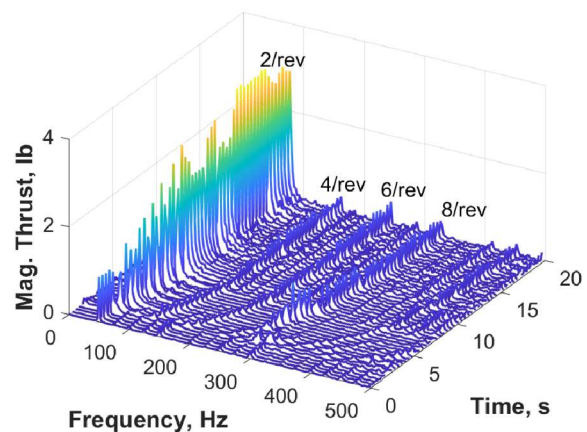


Figure 20. Waterfall plot for Rotor 2 isolated rotor thrust response to an RPM transient from 1,500 to 2,500 rpm. Pitch = -2 deg, and $q = 1.9$ lb/ft².

particularly those targeted at the Urban Air Mobility and Unmanned Aircraft Systems markets. The reconfigurable geometry of the MTB allows researchers to conduct trade studies and parametric investigations of multirotor aircraft performance without creating multiple wind tunnel models.

This paper summarized the design and capabilities of the MTB and described a small subset of the data that were gathered as part of the first wind tunnel test entry of the MTB in the U.S. Army 7- by 10-ft Wind Tunnel. The results shown give examples of the types of parametric studies that could be performed using the MTB. Once the complete data set has been validated, it will be made publicly available for researchers to use. NASA has already begun to use the data generated in the first MTB wind tunnel test to validate predictions of multirotor performance. Furthermore, the expectation is that the Multirotor Test Bed will become a key experimental capability for generating a wealth of multirotor validation data in the future.

REFERENCES

1. Russell, C., Willink, G., Theodore, C., Jung, J., and Glasner, B., "Wind Tunnel and Hover Performance Test Results for Multicopter UAS Vehicles", NASA/TM—2018-219758, February, 2018.
2. Russell, C., et al., "Multicopter UAS Performance Test 2" NASA/TM—TBD.
3. Chen, G., Nuñez, G., Russell, C., Avera, M., and Dotterweich, J., "Wind Tunnel Test Results for an Overlapped Quadrotor Configured UAS," AHS International 74th Annual Forum and Technology Display, Phoenix, AZ, May 14-17, 2018.
4. Conley, S., and Russell, C., "Comparing CFD Predictions of the Multirotor Test Bed with Experimental Results," Abstract submitted to VFS 76th Annual Forum and Technology Display, Montréal, QC, Canada, May 19-21, 2020.
5. Battey, L. and Russell, C., "Wind-Tunnel Testing a Small Isolated Folding Propeller," Vertical Flight Society 76th Annual Forum & Technology Display, Virginia Beach, VA, Oct. 6-8, 2020.
6. Conley, S. and Russell, C., "Mechanical Design of the Multirotor Test Bed," Vertical Flight Society Aeromechanics for Advanced Vertical Flight Technical Meeting, San Jose, CA, January 21-23, 2020.
7. Burnside, N.J. and Horne, W.C., "Development of Instrumentation and Methods for Time-Domain Measurement of Rotor-Type Sources in a Hard Wall Wind

ACKNOWLEDGEMENTS

The authors would like to acknowledge the contributions of the many people who helped make the MTB development and testing a success. In particular, from NASA, Gina Willink, Tom Norman, and Bill Warmbrodt provided invaluable guidance and assistance. The machine shop crews, led by Robert Kornienko and Vincent Derilo, machined the MTB hardware and provided guidance and helpful suggestions during the design process. Deividas Čelkys and Tomas Narbuntas provided operational support throughout the entire wind tunnel test. The first wind tunnel test of the MTB would not have been a success without the many hours put in by the U.S. Army 7- by 10-ft Wind Tunnel crew, particularly Gary Fayaud, Bruce Gesek, Steve Nance, Dan Pruyn, and Jiawei Toh. This work was primarily funded by NASA's Revolutionary Vertical Lift Technology (RVLT) Project, with seed funding from the NASA Ames FY18 Internal Research and Development Fund.

Tunnel." VFS Aeromechanics for Advanced Vertical Flight Technical Meeting, San Jose, CA, January 21-23, 2020.

8. Johnson, W. and Silva, S., "Observations from Exploration of VTOL Urban Air Mobility Designs," 7th Asian/Australian Rotorcraft Forum, Jeju Island, Korea, October 2018.
9. Langer, H.-J., Peterson, R., and Maier, T., "An Experimental Evaluation of Wind Tunnel Wall Correction Methods for Helicopter Performance," American Helicopter Society 52nd Annual Forum, Washington, D.C., June 4-6, 1996.
10. Healy, R., Misiorowski, M., and Gandhi, F., "A Systematic CFD-Based Examination of Rotor-Rotor Separation Effects on Interactional Aerodynamics for Large eVTOL Aircraft," Vertical Flight Society 75th Annual Forum & Technology Display, Philadelphia, PA, May 13-16, 2019.
11. Ventura Diaz, P. and Yoon, S., "Computational Study of NASA's Quadrotor Urban Air Taxi Concept," AIAA SciTech Forum 2020, Orlando, FL, January 6-10, 2020.
12. Schiller, N., Pascioni, K., and Zawodny, N., "Tonal Noise Control using Rotor Phase Synchronization," Vertical Flight Society 75th Annual Forum & Technology Display, Philadelphia, PA, USA, May 13-16, 2019.
13. Malpica, C. and Withrow-Maser, S., "Handling Qualities Analysis of Blade Pitch and Rotor Speed Controlled eVTOL Quadrotor Concepts for Urban Air Mobility," International Powered Lift Conference 2020, San Jose, CA, January 21-23, 2020.